






Research Article

Robust Flatness Tracking Control for the “DC/DC Buck Converter-DC Motor” System: Renewable Energy-Based Power Supply

Ramón Silva-Ortigoza ¹, **Alfredo Roldán-Caballero** ¹,
Eduardo Hernández-Márquez ², **José Rafael García-Sánchez** ³,
Magdalena Marciano-Melchor ¹, **Victor Manuel Hernández-Guzmán** ⁴,
and **Gilberto Silva-Ortigoza** ⁵

¹Instituto Politécnico Nacional, CIDETEC, Laboratorio de Mecatrónica & Energía Renovable, Ciudad de México 07700, Mexico

²Tecnológico Nacional de México, Instituto Tecnológico Superior de Poza Rica, Departamento de Ingeniería Mecatrónica, Veracruz 93230, Mexico

³Tecnológico Nacional de México, Tecnológico de Estudios Superiores de Huixquilucan, División de Ingeniería Mecatrónica, Estado de México 52773, Mexico

⁴Universidad Autónoma de Querétaro, Facultad de Ingeniería, Querétaro 76010, Mexico

⁵Benemérita Universidad Autónoma de Puebla, Facultad de Ciencias Físico Matemáticas, Puebla 72570, Mexico

Correspondence should be addressed to Ramón Silva-Ortigoza; rsilvao@ipn.mx

Received 29 June 2021; Accepted 8 September 2021; Published 14 October 2021

Academic Editor: Cutberto Romero Mel ndez

Copyright © 2021 Ramón Silva-Ortigoza et al. This is an open access article distributed under the Creative Commons Attribution License, which permits unrestricted use, distribution, and reproduction in any medium, provided the original work is properly cited.

The design of a robust flatness-based tracking control for the DC/DC Buck converter-DC motor system is developed in this paper. The design of the control considers the dynamics of a renewable energy power source that plays the role of the primary power supply associated with the system. The performance and robustness of the control is verified through simulations via MATLAB-Simulink when abrupt changes in some parameters of the system are taken into account. Also, experiments are performed by using a built prototype of the DC/DC Buck converter-DC motor system, a TDK-Lambda G100-17 programmable DC power supply, MATLAB-Simulink, and the DS1104 board from dSPACE. In this regard, the TDK-Lambda G100-17 is implemented with the aim of emulating photovoltaic panels through the solar array mode for generating the power supply of the system. Thus, both simulations and experiments show the effectiveness of the proposed control scheme.

1. Introduction

The rise of human population all around the globe has caused, as a direct consequence, an overdemand of energy consumption. According to [1], the world population will increase by almost 2.5 billion people by 2050. On the one hand, the demand of energy generated through fossil fuels leads to several environmental issues, such as global warming, acid rain, ozone layer depletion, among others [2]. In this context, the need of new research topics related to renewable energy, as an alternative to conventional energy, arises and is just where the research community should focus its efforts. On the other hand, it is well known that industry and transportation are the largest energy demand-consumption sectors around the world

[3] and both share one of the most highly used elements, the DC motor [4]. Because of this, the design of controls for DC motors fed by renewable energy power supplies turns out to be extremely relevant and important when the tracking or regulation tasks, associated with the angular velocity of the motor shaft, need to be solved. In this direction, it is usually to drive the velocity of the shaft by using pulse-width-modulation techniques. However, when using those techniques, some undesirable dynamic behavior emerges; that is, abrupt changes in voltage and current appear. It is stressed that this kind of variations can be reduced by implementing DC/DC power electronic converters. Such converters will attenuate the abrupt behavior due to the inductors and capacitors included in their design.

1.1. Related Works. According to the specialized literature, different topologies of DC/DC power electronic converters as drivers for DC motors have been proposed. The most important ones are Buck [5–40], Boost [41–48], Buck-Boost [49–54], Sepic [55, 56], Cuk [57], and Luo [58]. Nevertheless, as can be observed in all these contributions, the topology of the Buck converter-DC motor connection has attracted the greatest attention of the research community. The reason of this latter is as a result of its multiple applications and linear dynamic behavior. In this research, the Buck converter is used as driver for a DC motor. Thus, the corresponding review linked to the related works is presented below.

On the one hand, solutions associated with DC motors unidirectionally driven by DC/DC Buck converters to control their angular velocity are the following. Lyshevski, one of the pioneers in developing this type of systems, proposed a nonlinear PI control in [5]. Later, in [6] Ahmad et al. designed the PI, fuzzy PI, and LQR controls for the aforementioned system. In contrast to previous works, Linares-Flores et al. in [7] presented a velocity smooth starter based on flatness. Further, Bingöl and Paçacı in [8] applied a control based on neural networks. In another direction, Sira-Ramírez and Oliver-Salazar [9] exploited the active disturbance rejection and differential flatness concepts. The works by Hoyos et al. [10–13] reported an application of the zero average dynamics strategy and a fixed point induction control. Additionally, controls based on differential flatness were implemented by using hierarchical approaches [14–16], passivity and load torque estimation methods [17], derivative-free nonlinear Kalman filter [18], and successive loops [19]. Subsequently, a robust adaptive control based on sliding mode with dynamic surface was utilized by Wei et al. in [20]. Also, Hernández-Guzmán et al. in [21] introduced a control algorithm by using sliding mode plus PI controls. Likewise, Khubalkar et al. presented fractional-order PID controls in [22, 23] associated with dynamic particle swarm optimization (dPSO) and improved dPSO (IdPSO) techniques, respectively. Another research was exposed by Nizami et al. in [24], where a neuro-adaptive backstepping control using single-layer Chebyshev polynomials based neural network was exhibited. Recently, interesting contributions have been accomplished in [25–27]. Hanif et al. in [25] explained a safe experimentation dynamics algorithm for a data-driven piecewise affine PI control. Yang et al. in [26] studied a robust predictive control via a discrete-time reduced-order generalized proportional-integral (GPI) observer. Meanwhile, a fault detection scheme based on a combination of switching observer and bond graph method was addressed by Kasemi and Montazeri in [27]. More recently, Rigatos et al. in [28] used an adaptive neuro-fuzzy H-infinity control approach. And a continuous dynamic sliding mode control with high-order mismatched disturbance compensation was analyzed by Rauf et al. in [29]. Additionally, Guerrero et al. in [30] developed an active disturbance rejection control based on GPI observer for a DC motor driven by a parallel DC/DC Buck converter. Lastly, other important contributions, recently published, related to the connection of the DC/DC Buck power converter and DC motor have been reported in [31–35].

On the other hand, solutions associated with DC motors bidirectionally driven by DC/DC Buck converters are described next. A mathematical model and a sensorless passivity-based control with flatness were investigated by Silva-Ortigoza et al. in [36, 37], respectively. Likewise, Hernández-Márquez et al. considered two robust controls based on flatness [38]; the first control considers the system complete dynamics, whereas the second separates the dynamics of the system for using a hierarchical approach. Concerning this same system, an adaptive backstepping sliding-mode control integrated with Chebyshev neural network estimation was employed by Chi et al. in [39]. Another interesting study has been recently provided by Ismail and Elnady in [40], who described a new drive system for DC motor using multilevel DC/DC Buck converter circuit.

1.2. Discussion of Related Works, Motivation, and Contribution. In papers [5–40], different kinds of control schemes have been developed for both the regulation and the tracking tasks of DC motors fed by DC/DC Buck converters. Those control schemes considered the dynamics of the converter and the DC motor when the primary power supply of the converter, E , is obtained either by using a regulated power supply or by using static values. However, when the “DC/DC converter-DC motor” systems are fed through renewable energy power supplies, as presented in [39, 55, 56, 59], the dynamics of the power supply should be considered in the design of the controller with the aim of taking into account voltage and electric current variations related with such power supplies. A relevant approximation regarding the latter was reported by Gil-Antonio et al. in [60], where a flatness control was presented for the DC/DC Boost converter and also considered the dynamics associated with renewable energy sources. Thus, the contribution of this paper consists in developing a robust tracking control against power supply variations that may arise from the use of renewable energy sources in a DC/DC Buck converter-DC motor system. The feasibility and effectiveness of the proposed control are demonstrated via simulation studies and experimental tests through a built prototype. Particularly, this paper considers as the primary power supply the emulation of solar photovoltaic energy [61].

The rest of the paper is as follows. In Section 2, the generalities of the DC/DC Buck converter-DC motor system, where the dynamics associated with the renewable energy source is taken into consideration in the mathematical model, are presented, whereas the design of the differential flatness-based robust tracking control is described in Section 3. The simulations, which verify the effectiveness of the robust control, are presented in Section 4. Then, in Section 5, the system performance in closed loop is experimentally validated through tests by using a prototype of the system. Additionally, in Section 6, an assessment of the simulation and experimental results in closed loop is presented. Finally, the conclusions are given in Section 7.

2. DC/DC Buck Converter-DC Motor System

The circuit of the system under study is shown in Figure 1. This system is divided, for the purpose of this research, into three stages: a renewable energy power supply, a DC/DC Buck converter, and a DC motor. The *power supply*, due to its nature, is considered to be a function that depends on time (i.e., $E(t)$). The *converter* is built by using a transistor Q , a diode D , an inductor L , a capacitor C , and a load R . The input signal u allows the current i to flow through the inductor so that the voltage v can be generated in the load terminals. The *motor* is composed of a resistance R_a , an inductor L_a , a moment of inertia J , a friction coefficient b , and two electromechanical constants k_e and k_m . The flowing of current i_a through L_a allows the rotation of the motor shaft and, consequently, an angular velocity ω is originated.

By using the results reported in [21], the average mathematical model of the system depicted in Figure 1 is given as

$$\dot{x} = Ax + Bu_{av}, \quad (1)$$

where

$$A = \begin{bmatrix} 0 & -\frac{1}{L} & 0 & 0 \\ \frac{1}{C} & -\frac{1}{RC} & -\frac{1}{C} & 0 \\ 0 & \frac{1}{L_a} & -\frac{R_a}{L_a} & -\frac{k_e}{L_a} \\ 0 & 0 & \frac{k_m}{J} & -\frac{b}{J} \end{bmatrix}, \quad (2)$$

$$B = \begin{bmatrix} \frac{E(t)}{L} \\ 0 \\ 0 \\ 0 \end{bmatrix},$$

$$x = \begin{bmatrix} i \\ v \\ i_a \\ \omega \end{bmatrix},$$

with $u_{av} \in [0, 1]$.

3. Flatness-Based Tracking Control

In differential algebra, a system is considered to be differentially flat if all the state variables and the inputs

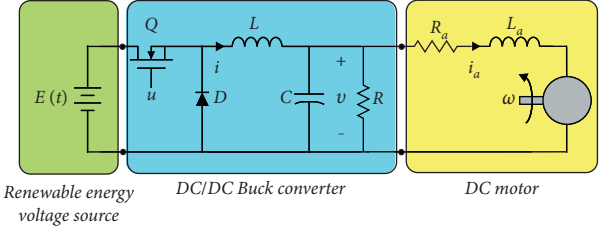


FIGURE 1: DC/DC Buck converter-DC motor system.

associated with vector state x and vector u , respectively, can be expressed in terms of a specific set of variables, called flat outputs, without using any kind of mathematical integration [62]. Based on [9], the flat output of the DC/DC Buck converter-DC motor system is determined by the angular velocity of the motor, that is, $y = \omega$. Thus, by performing some algebraic operations, the vector state and input can be strictly defined as functions of the flat output; this is

$$x = \begin{bmatrix} i(\omega) \\ v(\omega) \\ i_a(\omega) \\ \omega \end{bmatrix}, \quad (3)$$

$$u_{av} = u_{av}(\omega),$$

where

$$i(\omega) = \left[\frac{CJL_a}{k_m} \right] \omega^{(3)} + \left[\frac{bCL_aR + CJRR_a + JL_a}{k_mR} \right] \ddot{\omega} + \left[\frac{bL_a + JR + JR_a + bCRR_a + k_e k_m CR}{k_mR} \right] \dot{\omega} \quad (4)$$

$$+ \left[\frac{bR + bR_a + k_e k_m}{k_mR} \right] \omega,$$

$$v(\omega) = \frac{JL_a}{k_m} \ddot{\omega} + \left[\frac{bL_a + JR_a}{k_m} \right] \dot{\omega} + \left[\frac{bR_a}{k_m} + k_e \right] \omega, \quad (5)$$

$$i_a(\omega) = \frac{J}{k_m} \dot{\omega} + \frac{b}{k_m} \omega, \quad (6)$$

and

$$u_{av}(\omega) = \left[\frac{CJLL_a}{k_m E(t)} \right] \omega^{(4)} + \left[\frac{bCLL_aR + CJLRR_a + JLL_a}{k_m RE(t)} \right] \omega^{(3)} + \alpha \ddot{\omega} + \left[\frac{bLR + bLR_a + bL_aR + k_e k_m L + JRR_a}{k_m RE(t)} \right] \dot{\omega} \quad (7)$$

$$+ \left[\frac{bR_a + k_e k_m}{k_m E(t)} \right] \omega,$$

(7)

with

$$\alpha = \left[\frac{\text{bLL}_a + \text{JLR} + \text{JLR}_a + \text{bCLRR}_a + k_e k_m \text{CLR} + \text{JL}_a R}{k_m \text{RE}(t)} \right]. \quad (8)$$

On one hand, in order to avoid a division by zero in u_{av} (equation (7)) and the DC/DC Buck converter to operate adequately, then the voltage $E(t)$ must be considered strictly positive. On the other hand, the differential parameterization of the unidirectional DC/DC Buck converter-DC motor system, determined by equations (4)–(7), turns out to be similar to the case when the power supply is considered to be constant [7]. It is worth mentioning that in some other systems when the power supply is considered to be dynamic (i.e., as $E(t)$), in the control strategy appears explicitly $E(t)$ and its derivatives with respect to time. An example of this is the DC/DC Boost converter [60], whose average control u_{av} depends on $E(t)$ and $\dot{E}(t)$ when such a control is based on differential flatness.

After obtaining the differential parameterization of the DC/DC Buck converter-DC motor system (equation (1)), given by equations (4)–(7), the next step is to design the robust flatness-based tracking control. Hence, from equation (7), the following auxiliary control is proposed:

$$\omega^{(4)} = \mu. \quad (9)$$

The calculation of the auxiliary control μ is performed through equation (10) and achieves exponential asymptotic tracking of the trajectory ω , that is, $\omega \rightarrow \omega^*$, with ω^* being the desired angular velocity to be defined later:

$$\begin{aligned} 0 = & \left[\mu - \omega^{*(4)} \right] + k_4 \left[\omega^{(3)} - \omega^{*(3)} \right] + k_3 \left[\dot{\omega} - \dot{\omega}^* \right] \\ & + k_2 \left[\dot{\omega} - \dot{\omega}^* \right] + k_1 \left[\omega - \omega^* \right] + k_0 \int_0^t \left[\omega - \omega^* \right] d\tau. \end{aligned} \quad (10)$$

The integral component ensures zero static error in steady state and compensates the abrupt variations that can be generated in some parameters of the system. As can be observed, the error signal e has been defined as the difference between ω and ω^* . Thus, after introducing equation (10) in equation (9) in the frequency domain, the following is obtained:

$$P(s) = s^5 + k_4 s^4 + k_3 s^3 + k_2 s^2 + k_1 s + k_0, \quad (11)$$

where $\{k_0, k_1, k_2, k_3, k_4\}$ is the set of control parameters and has to be chosen so that the roots of the closed loop characteristic polynomial in the complex variable s ,

$$P_H(s) = [s + a] \left[s^2 + 2\zeta\omega_n s + \omega_n^2 \right]^2, \quad (12)$$

be a Hurwitz polynomial (i.e., a , ζ , and ω_n be positive constants). In this way, the set of control parameters are defined as

$$\begin{aligned} k_0 &= a\omega_n^4, \\ k_1 &= 4a\zeta\omega_n^3 + \omega_n^4, \\ k_2 &= 2a\omega_n^2 + 4a\zeta^2\omega_n^2 + 4\zeta\omega_n^3, \\ k_3 &= 4a\zeta\omega_n + 2\omega_n^2 + 4\zeta^2\omega_n^2, \\ k_4 &= a + 4\zeta\omega_n. \end{aligned} \quad (13)$$

Once the stability of subsystem equation (9) is ensured, the control signal u_{av} must be proposed. In this context, and with the aim of achieving that $\omega \rightarrow \omega^*$ in the DC/DC Buck converter-DC motor system (equation (1)), the control is now proposed by introducing equation (9) in equation (7); that is,

$$\begin{aligned} u_{av} = & \left[\frac{\text{CJLL}_a}{k_m E(t)} \right] \mu + \left[\frac{\text{bCLL}_a R + \text{CJLRR}_a + \text{JLL}_a}{k_m \text{RE}(t)} \right] \omega^{(3)} \\ & + \alpha \ddot{\omega} + \left[\frac{\text{bLR} + \text{bLR}_a + \text{bL}_a R + k_e k_m L + \text{JRR}_a}{k_m \text{RE}(t)} \right] \dot{\omega} \\ & + \left[\frac{\text{bR}_a + k_e k_m}{k_m E(t)} \right] \omega, \end{aligned} \quad (14)$$

where μ is obtained from equation (10) and is given by

$$\begin{aligned} \mu = & \omega^{*(4)} - k_4 \left[\omega^{(3)} - \omega^{*(3)} \right] - k_3 \left[\dot{\omega} - \dot{\omega}^* \right] \\ & - k_2 \left[\dot{\omega} - \dot{\omega}^* \right] - k_1 \left[\omega - \omega^* \right] - k_0 \int_0^t \left[\omega - \omega^* \right] d\tau. \end{aligned} \quad (15)$$

4. Simulations of the Flatness-Based Tracking Control

This section presents the implementation of the proposed control (equation (14)) in the DC/DC Buck converter-DC motor system described by equation (1). The performance and robustness of the differential flatness-based control is verified when the system is subjected to some abrupt changes in its parameters.

Figure 2 shows the block diagram that has been implemented in MATLAB-Simulink for acquiring the simulation results of the system in closed loop.

The reference input u_{av}^* and variables i^* , v^* , and i_a^* are obtained after substituting the desired angular velocity ω^* in the differential parameterization of the system, that is, in equations (4)–(7). The parameters of the DC/DC Buck converter and DC motor for obtaining the simulation results are

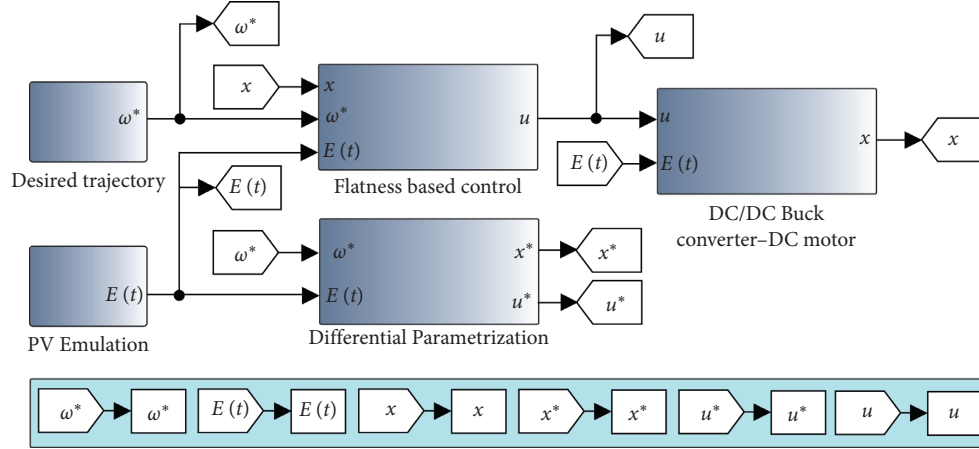


FIGURE 2: Block diagram associated with the implementation, in MATLAB-Simulink, of the flatness-based control in the DC/DC Buck converter-DC motor system.

$$\begin{aligned}
 L &= 286.5 \text{ mH}, \\
 C &= 114.4 \mu\text{F}, \\
 R &= 250 \Omega, \\
 L_a &= 2.22 \text{ mH}, \\
 k_m &= 120.1 \times 10^{-3} \frac{\text{N} \cdot \text{m}}{\text{A}}, \\
 R_a &= 0.965 \Omega, \\
 k_e &= 120.1 \times 10^{-3} \frac{\text{V} \cdot \text{s}}{\text{rad}}, \\
 J &= 118.2 \times 10^{-3} \text{ kg} \cdot \text{m}^2, \\
 b &= 129.6 \times 10^{-3} \frac{\text{N} \cdot \text{m} \cdot \text{s}}{\text{rad}}.
 \end{aligned} \tag{16}$$

While the gains of the control (k_0, k_1, k_2, k_3, k_4) are obtained after choosing and replacing the parameters $a = 2$, $\zeta = 0.707$, and $\omega_n = 900$ in equation (13).

4.1. Simulation Results. With the intention of verifying the performance of the proposed flatness-based control (equation (14)), the simulation results are now presented and

were developed in 4 different scenarios. For each one of these scenarios, two functions have been selected for the emulation of the renewable energy power supply associated with the system, $E(t)$:

- (i) The first two simulations consider the waveform reported by Gil-Antonio et al. in [60] (see Figure 3(a)) and is defined as

$$E(t) = 5[11.008 + 0.5504 \sin(5t) + 0.5848 \sin(10t)]. \tag{17}$$

- (ii) The last two simulations consider, as a function of time, the emulation of a photovoltaic module that is subjected to constant radiation [63, 64]. The behavior of such a module can be modeled (see Figure 3(b)) as

$$E(t) = 61(1 - e^{-30t}) + 0.5 \sin(100t) + 0.001. \tag{18}$$

Simulation 1. The first simulation contemplates the power supply described by equation (17). Also, the following desired angular velocity of the Bézier type is proposed:

$$\omega^*(t) = \bar{\omega}_i(t_i) + [\bar{\omega}_f(t_f) - \bar{\omega}_i(t_i)]\varphi(t, t_i, t_f), \tag{19}$$

where $\varphi(t, t_i, t_f)$ is defined by

$$\varphi(t, t_i, t_f) = \begin{cases} 0, & t \leq t_i, \\ 20 \left(\frac{t-t_i}{t_f-t_i} \right)^3 - 45 \left(\frac{t-t_i}{t_f-t_i} \right)^4 + 36 \left(\frac{t-t_i}{t_f-t_i} \right)^5 - 10 \left(\frac{t-t_i}{t_f-t_i} \right)^6, & t \in (t_i, t_f), \\ 1, & t \geq t_f. \end{cases} \tag{20}$$

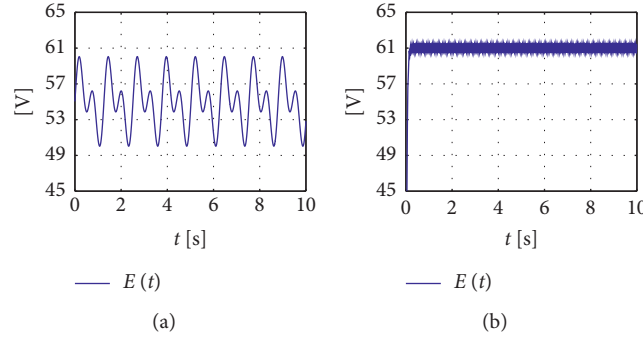


FIGURE 3: Renewable energy emulation of the power supply $E(t)$. (a) Waveform described by equation (17) and contains variations that could emerge from the usage of a renewable energy source. (b) Time-varying function proposed in equation (18) with variations that may appear in a photovoltaic module with constant radiation.

Thus, from equation (19), ω^* is smoothly interpolated from $\bar{\omega}_i(t_i)$ to $\bar{\omega}_f(t_f)$. Additionally, it has been selected that $\bar{\omega}_i = 0$ rad/s, $t_i = 2$ s, $\bar{\omega}_f = 13$ rad/s, and $t_f = 6$ s. In this simulation, whose results are depicted in Figure 4, the abrupt variations R_p are introduced in the load resistance R as follows:

$$R_p = \begin{cases} R & 0 \text{ s} \leq t < 3 \text{ s}, \\ 200\% R & 3 \text{ s} \leq t < 5 \text{ s}, \\ R & 5 \text{ s} \leq t < 7 \text{ s}, \\ 20\% R & 7 \text{ s} \leq t < 10 \text{ s}. \end{cases} \quad (21)$$

Simulation 2. In this simulation, the abrupt variations C_p are applied to the capacitance C and are defined as

$$C_p = \begin{cases} C & 0 \text{ s} \leq t < 3 \text{ s}, \\ 200\% C & 3 \text{ s} \leq t < 5 \text{ s}, \\ C & 5 \text{ s} \leq t < 7 \text{ s}, \\ 50\% C & 7 \text{ s} \leq t < 10 \text{ s}. \end{cases} \quad (22)$$

Here, for the power supply $E(t)$, the function proposed by Gil-Antonio et al. (equation (17)) and the desired angular velocity ω^* (equation (19)) are used again. Thus, the corresponding simulation results are presented in Figure 5.

Simulation 3. In this simulation, the power supply $E(t)$ of the DC/DC Buck converter-DC motor system is proposed to be the emulation of a photovoltaic module that is subjected to constant radiation. Likewise, as in the previous simulation results, the desired angular velocity corresponds to the one defined in equation (19). After taking into account the previous considerations and introducing the abrupt variations in load R given by R_p (equation (21)), the simulation results presented in Figure 6 are obtained.

Simulation 4. Lastly, in this simulation, the power supply $E(t)$ and the desired angular velocity ω^* are defined again as in equations (18) and (19), respectively. Hence, when the abrupt perturbations C_p (equation (22)) are applied in C , the behavior depicted in Figure 7 is achieved.

4.2. General Comments on the Simulation Results. The simulation results presented in Figures 4–7, associated with the numeric implementation of the flatness-based tracking control on the DC/DC Buck converter-DC motor system, show that the control objective is accomplished, that is, $\omega \rightarrow \omega^*$. The trajectory tracking task is achieved even when abrupt variations in R and C are taken into account. Moreover, the tracking task is also carried out even if abrupt variations appear in $E(t)$ as a consequence of using a renewable energy source. Note that the signal u_{av} compensates all variations in the power supply.

With the aim of demonstrating the performance of tracking control (equation (14)), the similarity of signals ω and ω^* is quantified through the following tracking error definition:

$$e_{Si} = \omega - \omega^*, \quad (23)$$

where subscript Si , with $i \in \{1, 2, 3, 4\}$, denotes the simulation test from which the error has been calculated. These errors are depicted within Figure 8, where it is easily observed that the dynamic behavior of the system in closed loop when $E(t)$ is defined as in equation (17), Simulations 1 and 2, is very similar when $E(t)$ is defined as in equation (18), Simulations 3 and 4. Such a similarity comes from the fact that the control u_{av} is robust enough to compensate all kinds of variations in $E(t)$ and, consequently, the angular velocity ω will be less affected by those variations. On the other hand, when perturbations in R are introduced into the system, the tracking errors e_{S1} and e_{S3} are larger than those associated with perturbations introduced through C , that is, the errors e_{S2} and e_{S4} . Those differences are due to the fact that current i is directly affected by any kind of change in load R . Because of this, the power delivered by the DC/DC Buck power converter-DC motor system must be greater to keep the same value of angular velocity ω .

5. Testbed and Closed Loop Experimental Results

In this section, the experimental results in closed loop are presented. With the aim of showing the effectiveness of the proposed control, given by equation (14), perturbations are

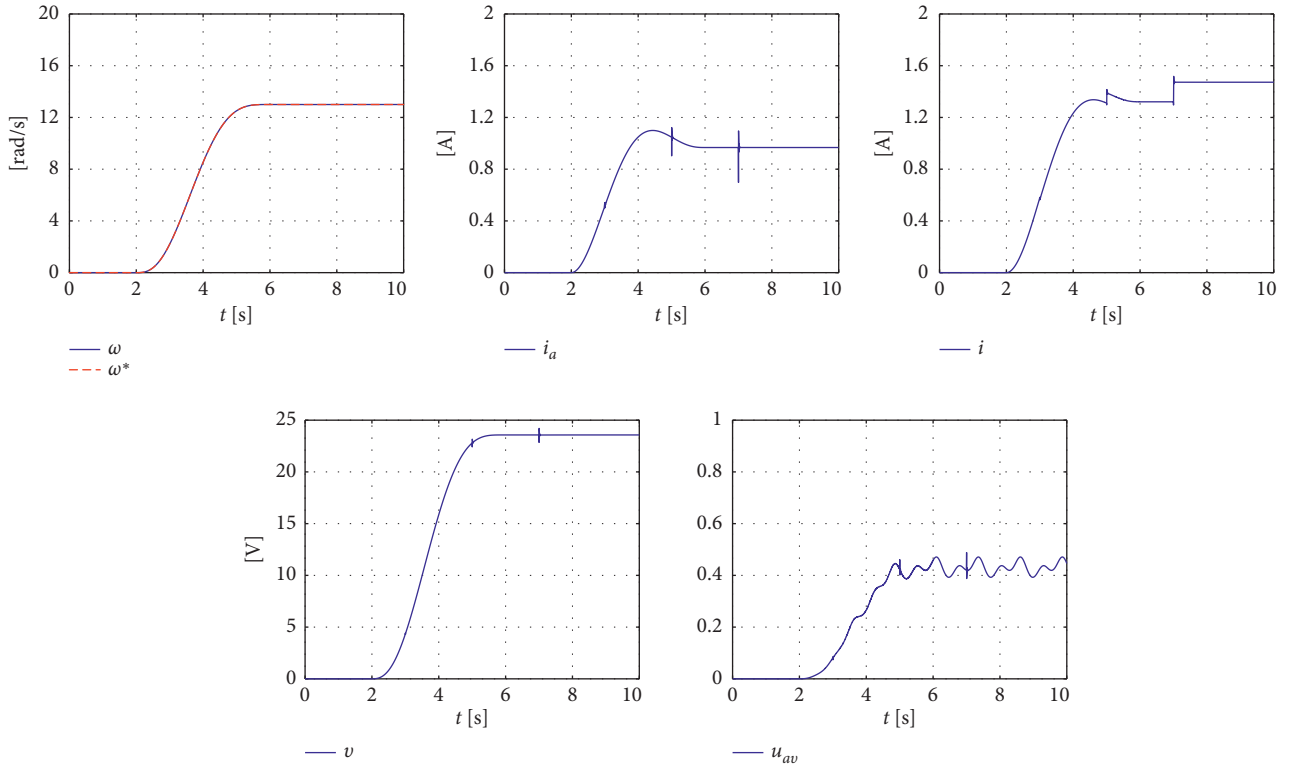


FIGURE 4: DC/DC Buck converter-DC motor system response when the time-variant waveform and abrupt variations are defined by equations (17) and (21), respectively.

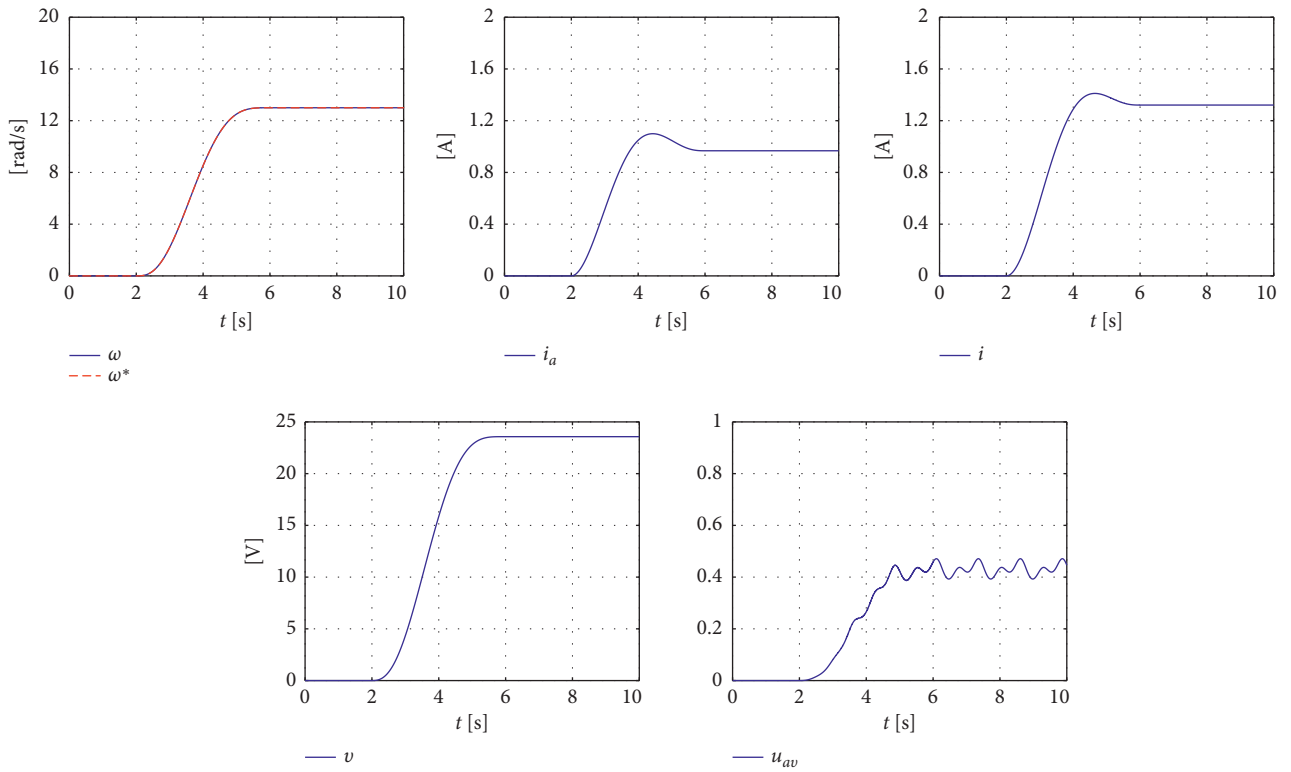


FIGURE 5: Response of the DC/DC Buck converter-DC motor system when the time-variant waveform and the abrupt variations are defined by equations (17) and (22), respectively.

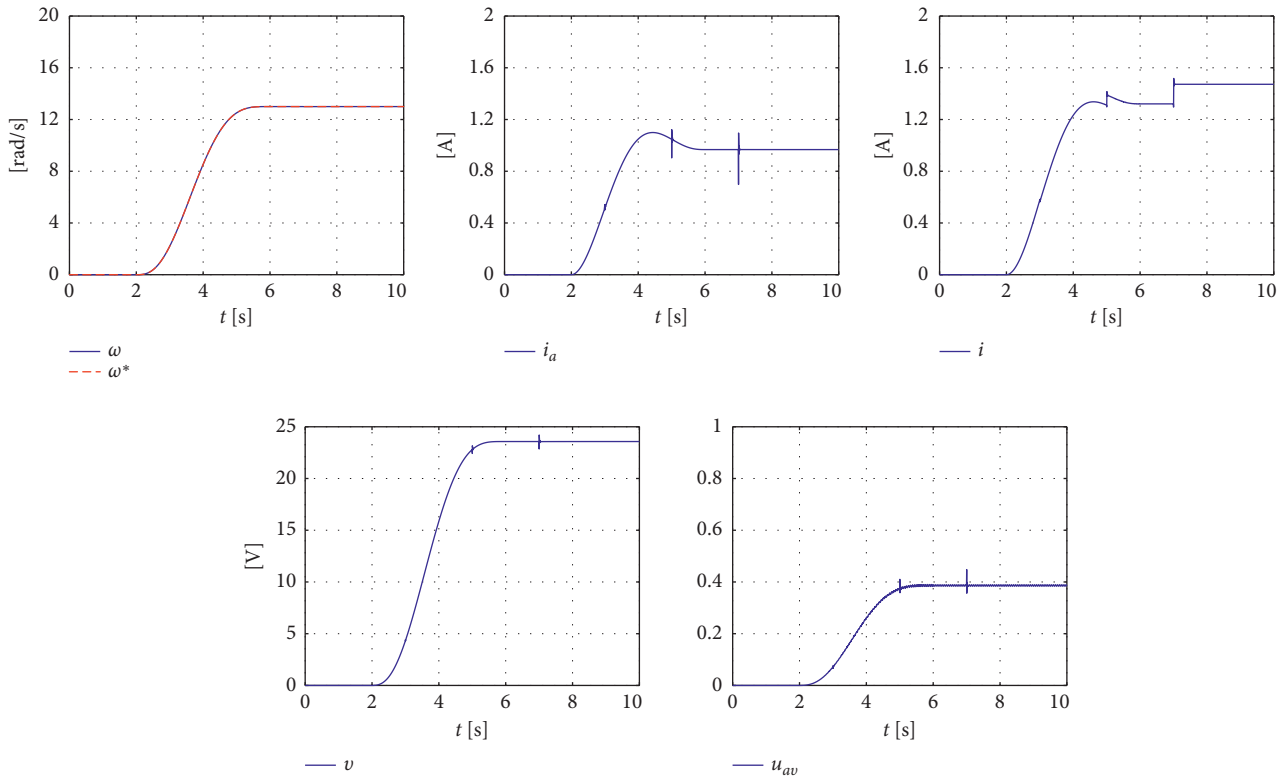


FIGURE 6: Time-response of the DC/DC Buck converter-DC motor system when using the waveform (equation (18)) and abrupt variations (equation (21)) in R .

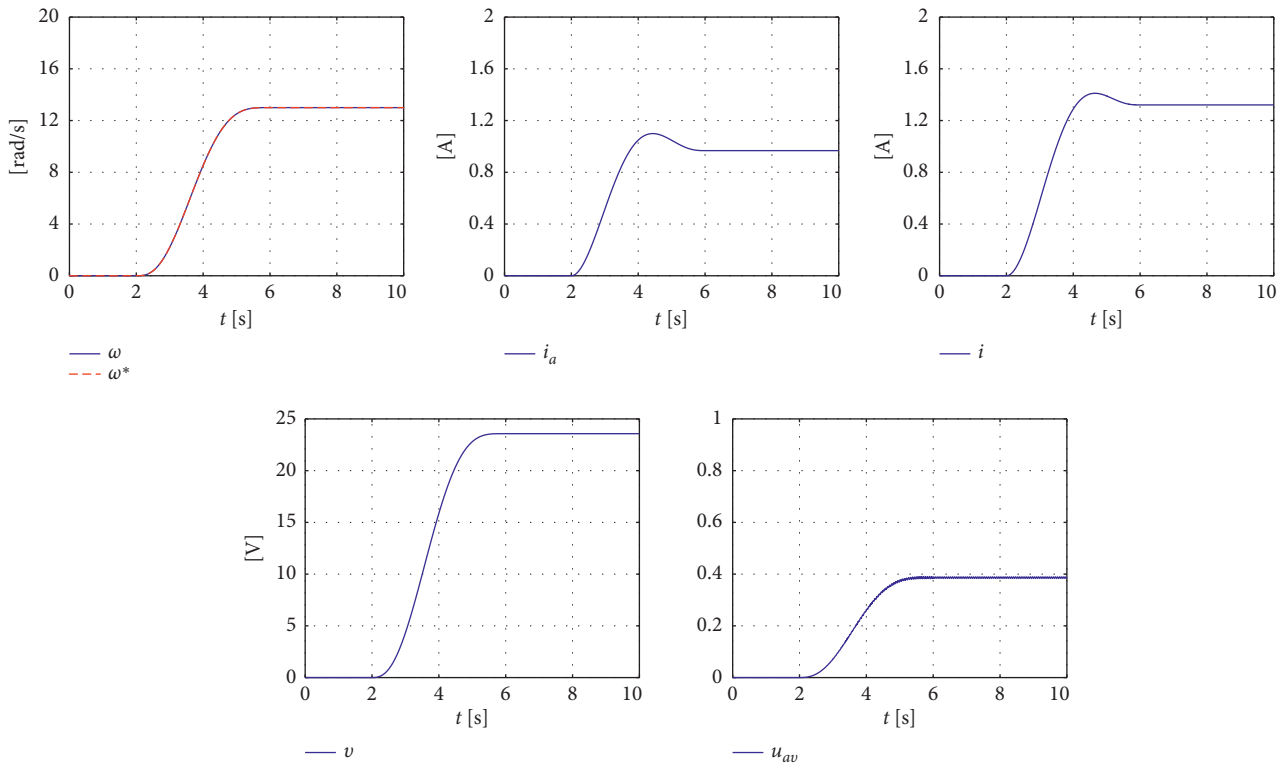


FIGURE 7: Dynamic behavior of the DC/DC Buck converter-DC motor system when $E(t)$ is given by equation (18) and when the abrupt changes (equation (22)) are introduced in C .

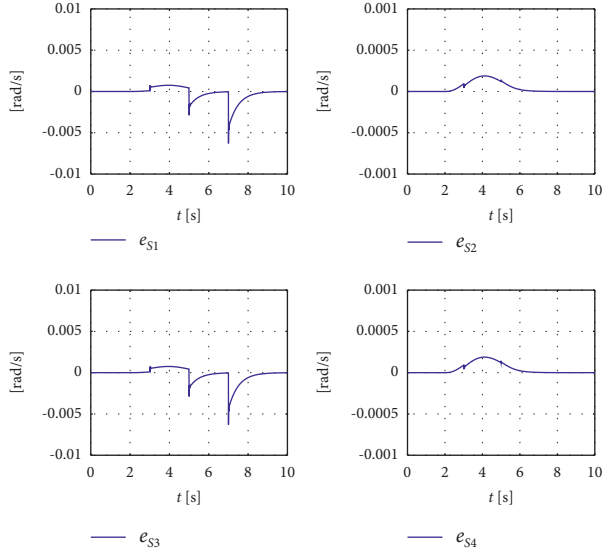


FIGURE 8: Angular velocity tracking errors obtained from the simulation results depicted in Figures 4–7 when abrupt variations are applied in parameters R and C of the DC/DC Buck converter-DC motor system and when $E(t)$ emulates a renewable energy power supply given by equations (17) and (18).

considered in some parameters of the DC/DC Buck converter-DC motor system.

5.1. Experimental Testbed. The general diagram of the experimental testbed, for implementing the design control on the DC/DC Buck converter-DC motor system that considers the emulation of renewable energy, is shown in Figure 9.

The blocks composing the experimental testbed, depicted in Figure 9, are as follows:

- (i) *Desired Trajectory and Reference Variables.* In this block, the desired trajectory ω^* and the reference variables i^* , v^* , i_a^* , and u_{av} , obtained when ω^* is replaced in equations (4)–(7), are programmed through MATLAB-Simulink.
- (ii) *Flatness-Based Control.* Here, the flatness-based control (equation (14)) is programmed also via MATLAB-Simulink. It is worth mentioning that such a control requires only the information associated with the flat output of the system, ω , and the power supply $E(t)$. The gains of the control scheme $(k_0, k_1, k_2, k_3, k_4)$, previously declared, are obtained after the parameters $a = 1$, $\zeta = 10$, and $\omega_n = 1200$ are introduced in equation (13).
- (iii) *Board and Signal Conditioning Circuit.* The connection of the DC/DC Buck converter-DC motor system along with the DS1104 board from dSPACE is realized in this block. For such an aim, the signals $E(t)$ and v are measured through two Tektronix P5200 A voltage probes, whereas i and i_a are measured by using two Tektronix A622 current probes, and ω is measured via an E6B2-CWZ6C encoder. The signal conditioning is executed with

blocks SC. Also, the control signal u , allowing the appropriate commutation of transistor Q , is obtained after the signal u_{av} is modulated through a PWM port of the DS1104 board. The electrical isolation between the DS1104 board and the power system is achieved by implementing a TLP250 photocoupler.

- (iv) *DC/DC Buck Converter-DC Motor.* This block corresponds to the built DC/DC Buck converter-DC motor system prototype. Here, a TDK-Lambda G100-17 programmable DC power supply is used to provide the signal $E(t)$. With such a power supply, it is possible to generate several DC arbitrary waveforms. As a matter of fact, it is possible also to emulate photovoltaic panels through the solar array mode option. Regarding the prototype, the parameters of the DC/DC Buck converter-DC motor system built are exactly the same as those used in simulations and are given by equation (16).

Additionally, a photograph of the experimental testbed associated with the DC/DC Buck converter-DC motor system, depicted in Figure 9, is shown in Figure 10.

5.2. Experimental Results in Closed Loop. In correspondence to the four different scenarios for which the simulations of the system in closed loop were obtained (see Section 1.1), here, the experimental results linked to those simulations are presented.

As it was previously stated, the emulation of the renewable energy power supply $E(t)$ was achieved by proposing the following two functions:

- (i) For the first two experiments, the wave form $E(t)$ was proposed as the one reported by Gil-Antonio et al. in [60], whose behavior is depicted in Figure 3(a); this is,

$$E(t) = 5[11.008 + 0.5504 \sin(5t) + 0.5848 \sin(10t)]. \quad (24)$$

The experimental implementation of equation (24) was carried out by programming the TDK-Lambda G100-17 power supply. Thus, the waveform of signal $E(t)$ had the form presented in Figure 11(a).

- (ii) Regarding the third and fourth experiments, the waveform of $E(t)$ was generated by emulating a photovoltaic module subjected to constant radiation and whose dynamic behavior was shown in Figure 3(b). The mathematical model for such an $E(t)$ was given by equation (18); that is,

$$E(t) = 61(1 - e^{-30t}) + 0.5 \sin(100t) + 0.001. \quad (25)$$

In this case, the experimental implementation of equation (25) was achieved through the solar array simulator of the TDK-Lambda G100-17 power supply by selecting the TS-S425 solar panel, whose

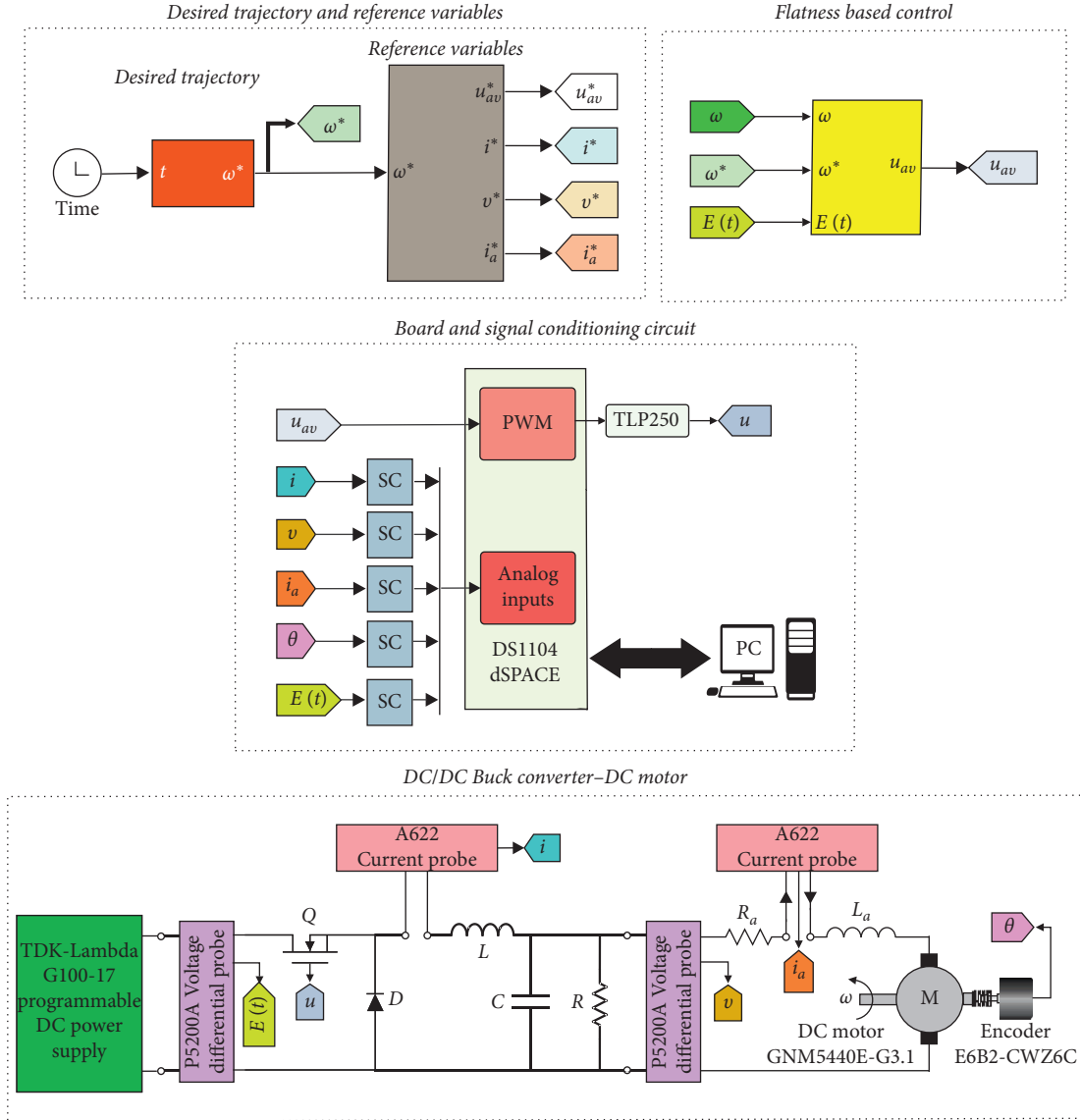


FIGURE 9: Diagram of the experimental testbed associated with the DC/DC Buck converter-DC motor system.

V-I graphic and dynamic behavior are depicted in Figures 11(b) and 11(c), respectively.

Experiment 1. In correspondence to the results of Simulation 1 (see Figure 4), in this section, the experimental results linked to those simulations are presented. Thus, for $E(t)$, the experimental realization of equation (24), depicted in Figure 11(a), is introduced, whereas the angular velocity of the Bézier type (equation (19)), previously defined, is used. That is,

$$\omega^*(t) = \bar{\omega}_i(t_i) + [\bar{\omega}_f(t_f) - \bar{\omega}_i(t_i)]\varphi(t, t_i, t_f), \quad (26)$$

with $\varphi(t, t_i, t_f)$ defined by equation (20). Then, from equation (26), the signal ω^* smoothly interpolates from $\bar{\omega}_i$ to $\bar{\omega}_f$ in t_i and t_f , respectively. In this way, the experimental results associated with perturbations R_p equation (27) are shown in Figure 12.

$$R_p = \begin{cases} R & 0 \text{ s} \leq t < 3 \text{ s}, \\ 200\% R & 3 \text{ s} \leq t < 5 \text{ s}, \\ R & 5 \text{ s} \leq t < 7 \text{ s}, \\ 20\% R & 7 \text{ s} \leq t < 10 \text{ s}. \end{cases} \quad (27)$$

Experiment 2. In regard with the results of Simulation 2 (see Figure 5), in this section, the experimental results associated with those simulations are presented.

In this experiment, the waveform for $E(t)$ shown in Figure 11(a), representing a renewable energy source, is again implemented via the TDK-Lambda G100-17 programmable DC power supply. Then, after using the desired angular velocity ω^* (equation (26)) and introducing the variations C_p (equation (28)) in capacitance C of the DC/DC Buck converter, the obtained results are depicted in Figure 13.

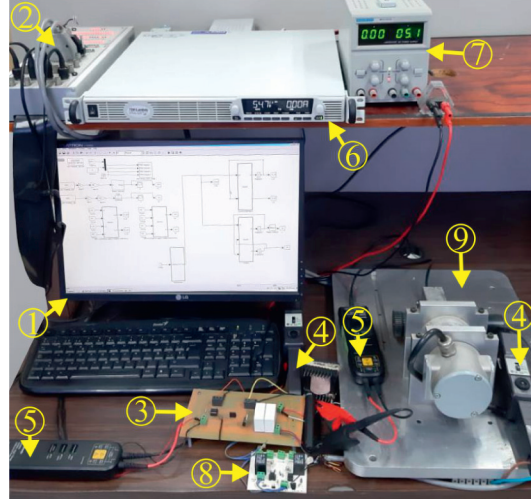


FIGURE 10: Photograph of the testbed associated with the DC/DC Buck converter-DC motor system. (1) PC, (2) DS1104 board from dSPACE, (3) DC/DC Buck converter, (4) Tektronix A622 current probes, (5) Tektronix P5200A voltage probes, (6) TDK-Lambda G100-17 programmable DC power supply, (7) power supply of the instrumentation stage, (8) electronic board to apply perturbations, and (9) DC motor.

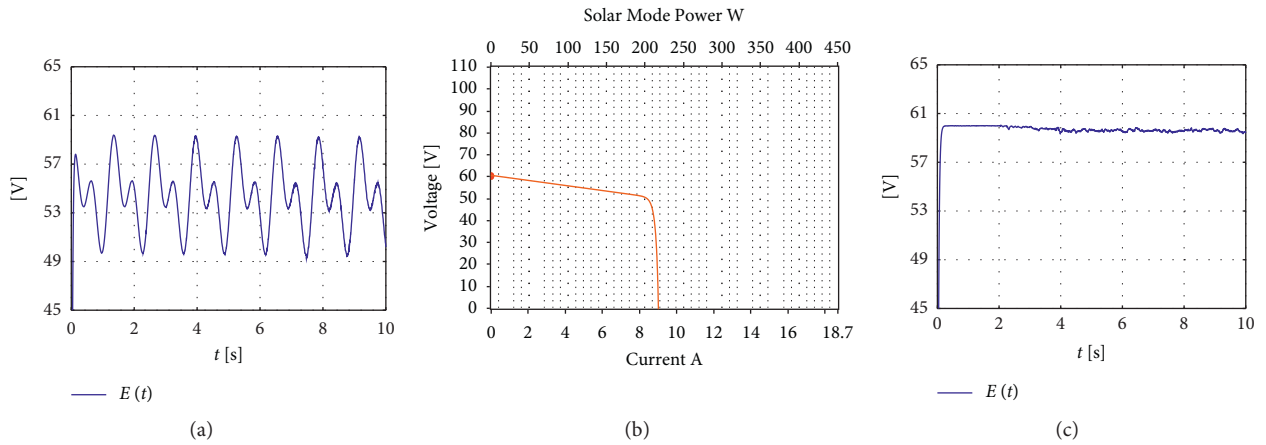


FIGURE 11: Renewable energy emulation of $E(t)$ generated via the TDK-Lambda G100-17 programmable DC power supply. (a) Experimental realization of the waveform (equation (24)) that contains some variations that could arise from the usage of a renewable energy source. Experimental implementation when the programmable DC power supply emulates the behavior of solar panels with constant radiation (equation (25)). (b) V-I curve of the TS-S425 solar panel and (c) dynamic behavior of the TS-S425 solar panel.

$$C_p = \begin{cases} C & 0 \text{ s} \leq t < 3 \text{ s}, \\ 200\% C & 3 \text{ s} \leq t < 5 \text{ s}, \\ C & 5 \text{ s} \leq t < 7 \text{ s}, \\ 50\% C & 7 \text{ s} \leq t < 10 \text{ s}. \end{cases} \quad (28)$$

Experiment 3. In this section, the experimental results linked to the results of Simulation 3 (see Figure 6) are presented.

In order to obtain the experimental results presented in Figure 14, the power supply $E(t)$ feeds the system with the waveform shown in Figure 11(c), corresponding to the emulation of a signal delivered by a solar panel with constant radiation. Such an $E(t)$ is generated through the TDK-

Lambda G100-17 programmable DC power supply by using its solar array mode, as a result of having used the solar panel TS-S425 for the experimental implementation of equation (25). Likewise, the results presented in Figure 14 consider the desired angular velocity of the Bézier type (equation (26)) and perturbations R_p (equation (27)) for the load R .

Experiment 4. Lastly, this section shows the experimental results associated with Simulation 4 (see Figure 7). In this experiment, the power supply $E(t)$ feeds the system with a similar waveform as the one used in Experiment 3. Such a waveform is depicted in Figure 11(c) and generated through the solar panel TS-S425 of the programmable DC power supply. Then, after using ω^* (equation (26)) and introducing perturbations C_p (equation (28)) in capacitance C of the

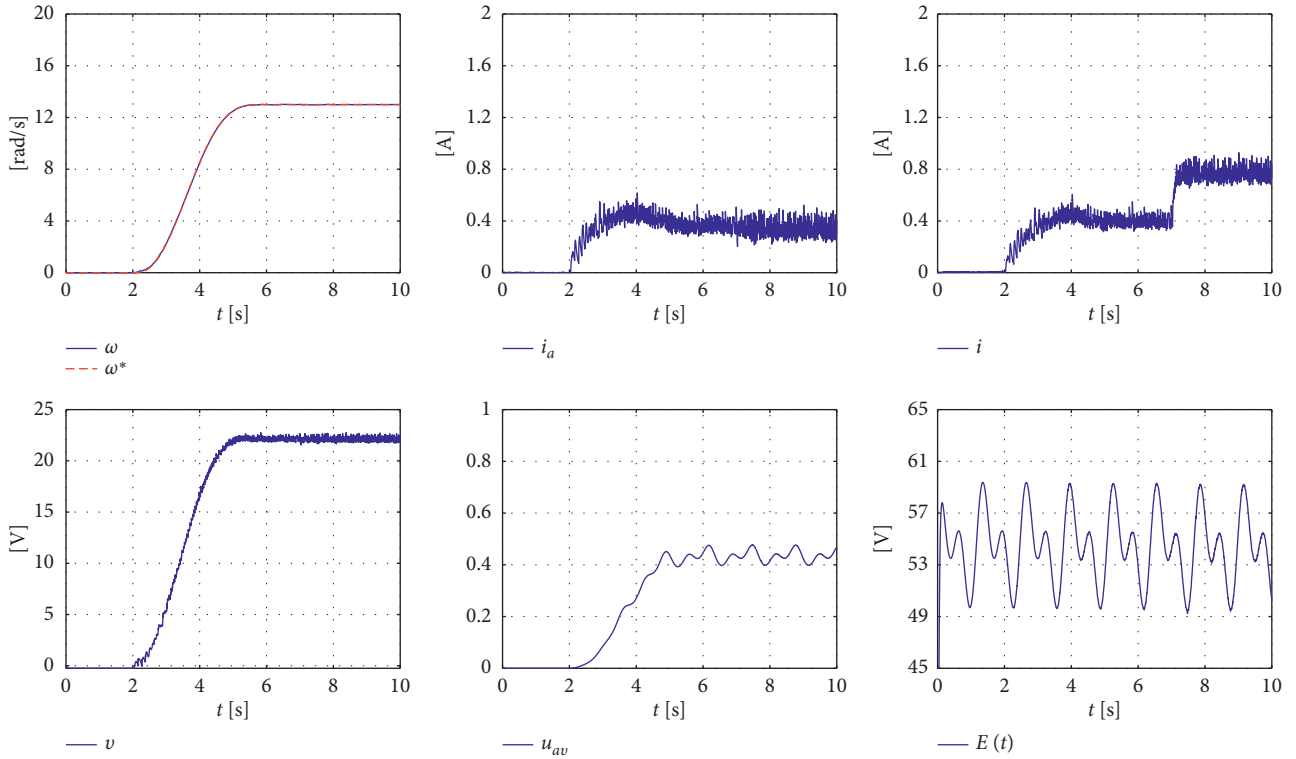


FIGURE 12: Dynamic response of the DC/DC Buck converter-DC motor system when $E(t)$, given by equation (24), is experimentally implemented through the TDK-Lambda G100-17 power supply and when the abrupt variations (equation (27)) are considered in R .

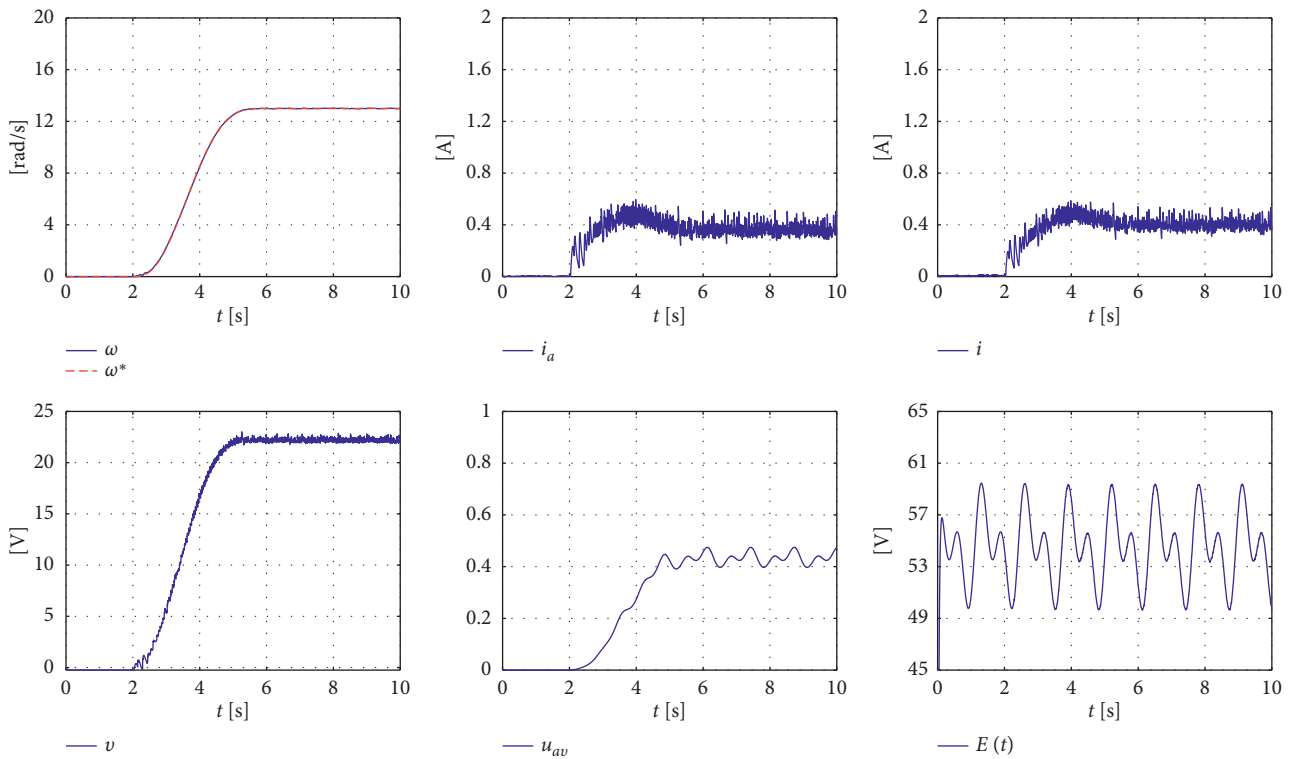


FIGURE 13: Dynamic response of the DC/DC Buck converter-DC motor system when $E(t)$ is defined as in equation (24), experimentally implemented through the TDK-Lambda G100-17 programmable power supply, and considering variations equation (28) in C .

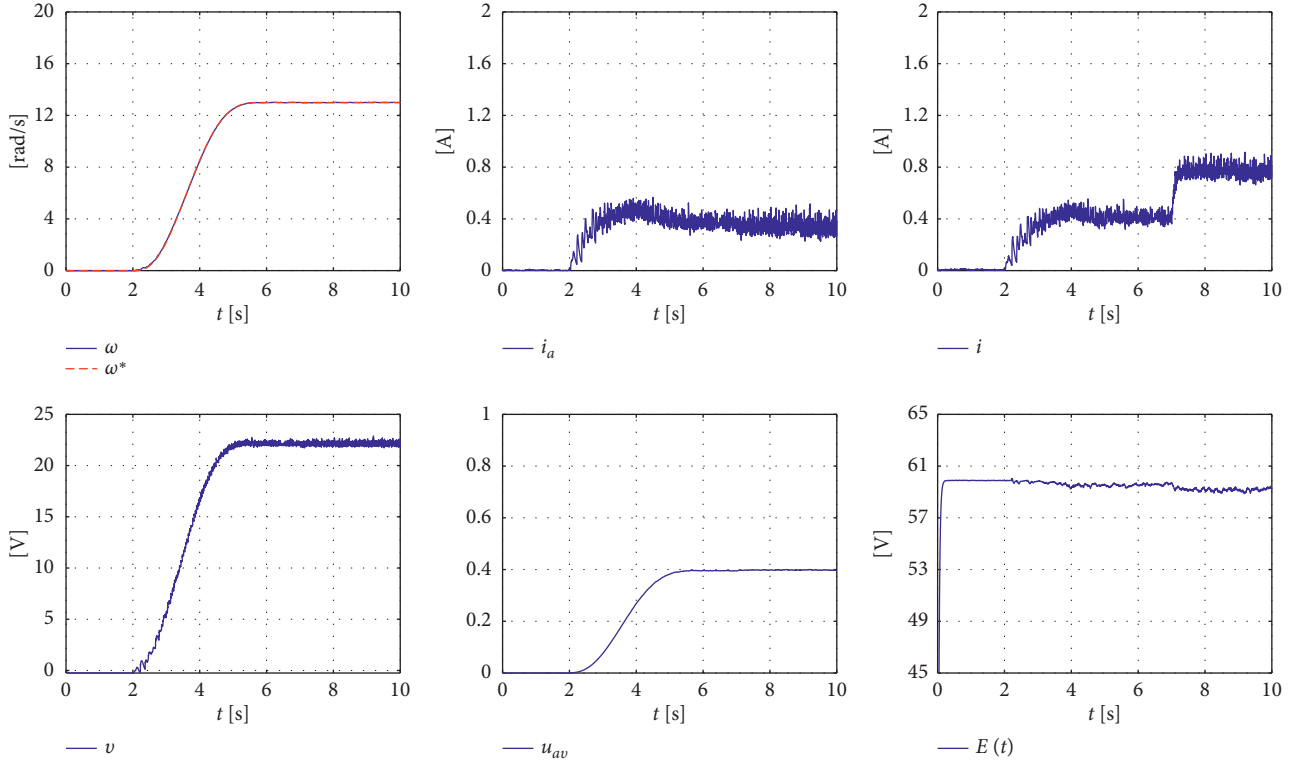


FIGURE 14: Experimental results of the DC/DC Buck converter-DC motor system in closed loop when $E(t)$ is given by equation (25) and carried out through the TDK-Lambda G100-17 power supply via the solar panel TS-S425, and the variations equation (27) are taken into account in R .

Buck converter, the obtained experimental results are depicted in Figure 15.

5.3. General Comments on the Experimental Results. In correspondence to the results of the numeric implementation presented in Section 1.1, the experimental implementation associated with the control scheme based on differential flatness (equation (14)) was carried out and the obtained results are shown in Figures 12–15. The experimental realization was executed by using a built DC/DC Buck converter-DC motor system, where variations on the power supply $E(t)$, which could emerge from the usage of renewable energy sources, were considered. Similar to simulation results, the experimental ones demonstrated that $\omega \rightarrow \omega^*$ when $E(t)$ is described by equations (24) and (25) and even when abrupt variations (equations (27) and (28)) are introduced in parameters R and C , respectively.

The experimental results depicted in Figures 12 and 14 show a bigger variation in current i , when perturbations in load R (equation (27)) are taken into account, with respect to those presented in Figures 13 and 15, associated with perturbations C (equation (28)). Also, it is worth noting that voltage $E(t)$ in the experimental results presented in Figures 14 and 15 drops when the load of the system rises. Such a voltage drop is due to an increase in current, which represents a natural behavior in solar panels. In this direction, the experimental results presented in Figures 14 and 15 were obtained by generating $E(t)$ (equation (25)) through the solar panel TS-S425 (see Figures 11(b) and 11(c)) of the

TDK-Lambda G100-17 programmable power supply. On the other hand, the tracking error related to the control based on differential flatness (equation (14)) needs to be quantified, that is, the difference between ω and ω^* . Thus, in correspondence to the definition given by equation (23), the tracking error of the experimental results is defined as

$$e_{Ej} = \omega - \omega^*, \quad (29)$$

where subscript Ej , with $j \in \{1, 2, 3, 4\}$, denotes the experimental result from which the error has been calculated. These errors are depicted within Figure 16, and as can be observed the tracking errors of the experimental results are larger in magnitude in comparison with the simulation ones shown in Figure 8. The difference between the tracking errors of the simulation results and the experimental results is because the mathematical model of the system does not take into account some dynamics, such as the internal resistance of the solid-state devices, heat losses, nonlinearities, among others. Nevertheless, the tracking errors associated with the experimental results are small enough regarding the angular velocity magnitude. Thus, it can be concluded that the control objective is satisfactorily achieved, that is, $\omega \rightarrow \omega^*$.

6. Assessment of the Simulation and Experimental Results

Lastly, this section presents a direct visual comparison between the simulation and experimental results associated

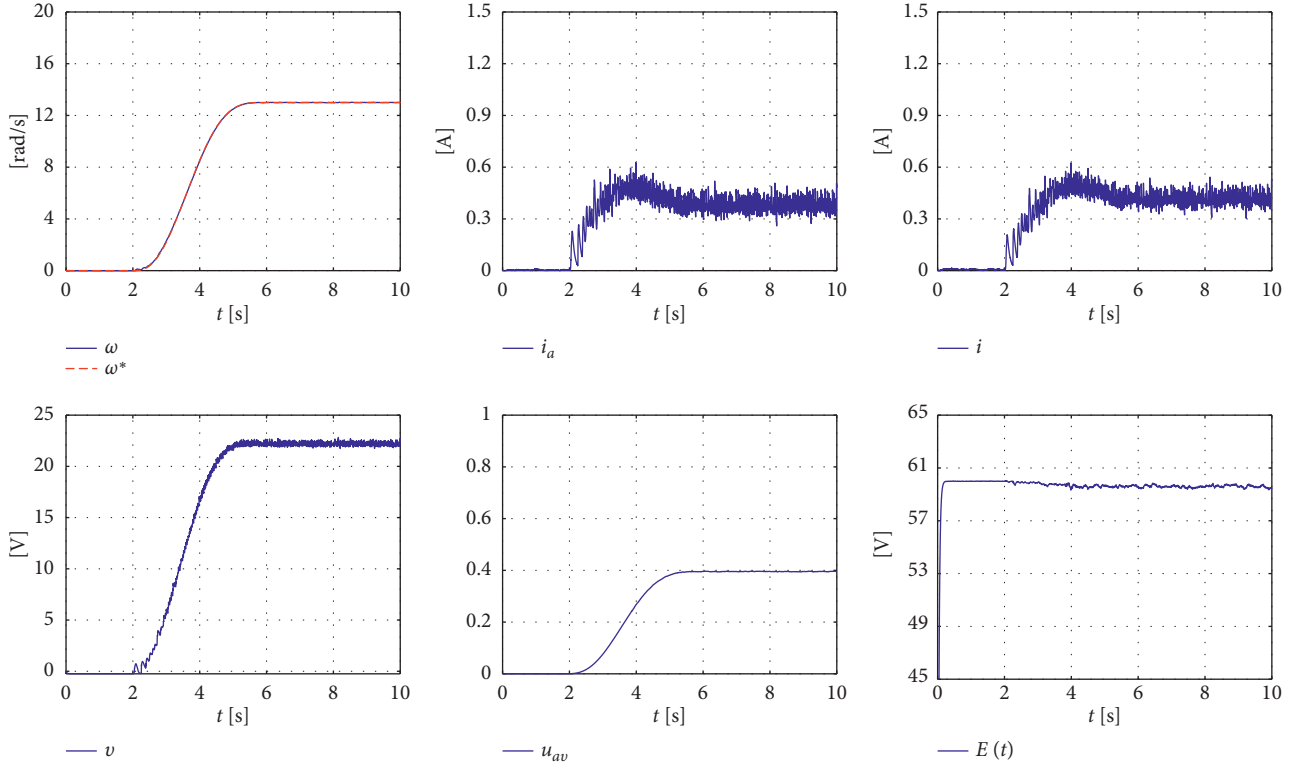


FIGURE 15: Experimental results of the DC/DC Buck converter-DC motor system in closed loop when $E(t)$ (equation (25)) is generated through the TDK-Lambda G100-17 programmable power supply, via the solar panel TS-S425, and the perturbations (equation (28)) are imposed in C .

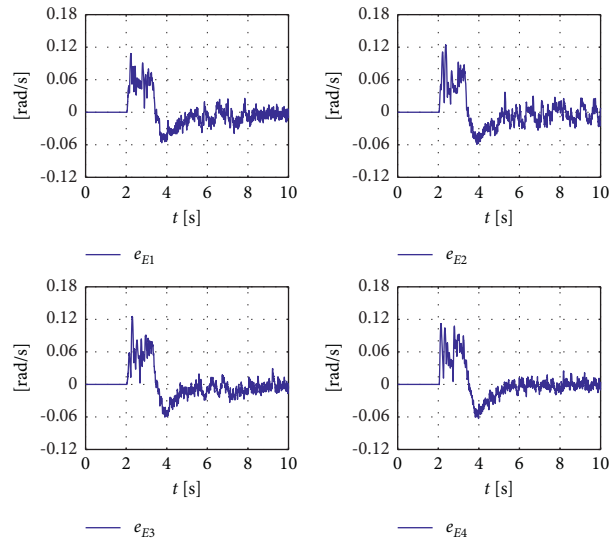


FIGURE 16: Angular velocity tracking errors obtained from the experimental results shown in Figures 12–15 when abrupt variations are considered in parameters R and C of the DC/DC Buck converter and $E(t)$ emulates a renewable energy power supply. The plotted results associated with e_{E1} and e_{E2} are achieved when the experimental implementation of $E(t)$ (equation (24)) is programmed through the TDK-Lambda G100-17 power supply, while the plotted results related to e_{E3} and e_{E4} are obtained when the experimental implementation of $E(t)$ (equation (25)) is realized via the solar panel TS-S425 of the TDK-Lambda G100-17 power supply.

with ω . Such a comparison is realized through a visual assessment that is achieved by including, simultaneously, the simulation results and the corresponding experimental ones in the same graphic. This is executed with the aim of

highlighting the good performance of the tracking control based on differential flatness.

To carry out the comparison, the variables ω_{S1} , ω_{S2} , ω_{S3} , and ω_{S4} are defined as the angular velocities previously

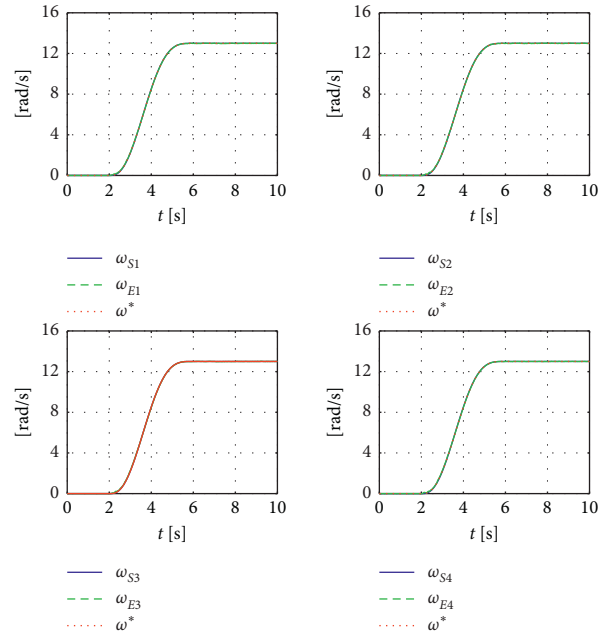


FIGURE 17: Assessment of the trajectory tracking task for the angular velocity ω associated with the DC/DC Buck converter-DC motor system, via a direct visual comparison between the simulation and experimental results.

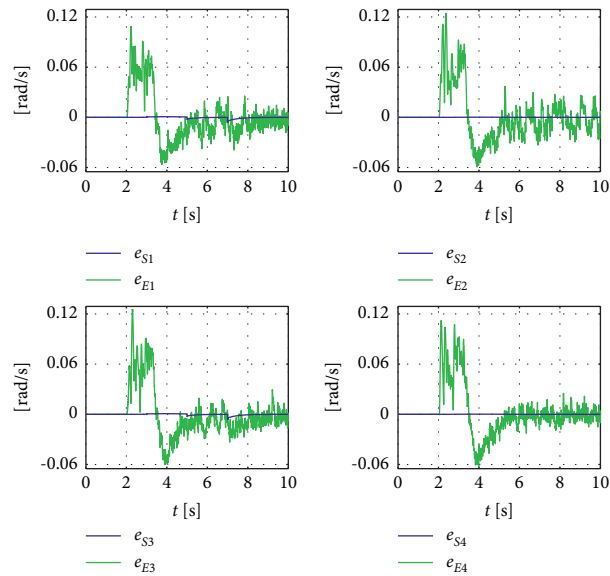


FIGURE 18: Tracking errors of the system in closed loop for ω . In these graphics, the tracking errors associated with the simulation results are denoted as e_{S1} , e_{S2} , e_{S3} , and e_{S4} , while the tracking errors related to the experimental results are represented by e_{E1} , e_{E2} , e_{E3} , and e_{E4} .

obtained at simulation level and shown in the first graphic of Figures 4–7, respectively. Also, the variables ω_{E1} , ω_{E2} , ω_{E3} , and ω_{E4} are now defined as the angular velocities previously obtained at experimental level and depicted in the first graphic of Figures 12–15, respectively. Thus, after having redefined the simulation and experimental results for the angular velocity, in Figure 17, the direct visual comparison between the simulation and experimental results for ω is presented.

In Figure 17, it is observed that the experimental results are very similar to their corresponding simulation ones. This is confirmed through the graphics of the tracking errors for

ω depicted in Figure 18. Such a figure emerges as a result of overlapping the plots associated with the simulation closed loop tracking errors e_{S_i} (shown in Figure 8) and the plots related to the experimental closed loop tracking errors e_{E_j} (shown in Figure 16). Thus, again, it can be concluded that the control objective is satisfactorily achieved, i.e., $\omega \rightarrow \omega^*$.

7. Conclusion

This paper considered, for the first time, the dynamics of the primary power supply in the design of a robust tracking control for the DC/DC Buck converter-DC

motor system. Particularly, the emulation of solar photovoltaic energy was introduced in this work. Also, the flatness property associated with the mathematical model was exploited with the aim of describing the control signal in terms of the flat output, conveniently determined by the angular velocity of the motor shaft, allowing the design of a robust tracking control. The robustness of the control was verified, via simulations in MATLAB-Simulink, when abrupt changes are considered in some parameters of the system.

The performance and robustness of the control was verified via simulations in MATLAB-Simulink when abrupt changes were considered in some parameters of the system. While the experimental implementation was carried out on a built prototype of the DC/DC Buck converter-DC motor system, a TDK-Lambda G100-17 programmable DC power supply, MATLAB-Simulink, and the DS1104 board from dSPACE. The TDK-Lambda G100-17 power supply allowed to generate DC arbitrary waveforms and to emulate solar panels for $E(t)$. It is worth mentioning that the approach presented in this paper can be applied in many types of systems whose power supply is based on renewable energy sources. Thus, it would not be necessary to redesign the control strategy when changing the primary power supply.

Finally, motivated by the obtained results of this research, the design of controls that considers the important problem of active disturbance rejection [65, 66] and applications in mobile robotics and subactuated systems are considered as future work.

Data Availability

The data used to support the findings of this study are available from the corresponding author upon request.

Conflicts of Interest

The authors declare that the research was conducted in the absence of any commercial, financial, or personal relationships that could be construed as a potential conflict of interests.

Acknowledgments

This work was supported by the Instituto Politécnico Nacional, México. The work of R. Silva-Ortigoza and M. Marciano-Melchor was supported by the SNI-México and IPN Programs EDI and SIBE. The work of A. Roldán-Caballero was supported by the CONACYT-México and BEIFI scholarships. The work of E. Hernández-Márquez, J. R. García-Sánchez, V. M. Hernández-Guzmán, and G. Silva-Ortigoza was supported by the SNI-México.

References

- [1] D. M. Kammen and D. A. Sunter, "City-integrated renewable energy for urban sustainability," *Science*, vol. 352, no. 6288, pp. 922–928, 2016.
- [2] I. Dincer, "Renewable energy and sustainable development: a crucial review," *Renewable and Sustainable Energy Reviews*, vol. 4, no. 2, pp. 157–175, 2000.
- [3] J. Twidell and T. Weir, *Renewable Energy Resources*, Taylor & Francis, London, U.K., 3rd edition, 2015.
- [4] J. F. Gieras, *Permanent Magnet Motor Technology: Design and Applications*, CRC Press, Boca Raton, FL, USA, 3rd edition, 2010.
- [5] S. E. Lyshevski, *Electromechanical Systems, Electric Machines, and Applied Mechatronics*, CRC Press, Boca Raton, FL, USA, 2000.
- [6] M. A. Ahmad, R. M. T. Raja-Ismail, and M. S. Ramli, "Control strategy of buck converter driven DC motor: a comparative assessment," *Australian Journal of Basic and Applied Sciences*, vol. 4, no. 10, pp. 4893–4903, 2010.
- [7] J. Linares-Flores, A. Antonio-García, and A. Orantes-Molina, "Arranque suave para un motor de CD a través de un convertidor reductor CD-CD," *Ingeniería: Investigación y Tecnología*, vol. 12, no. 2, pp. 137–148, 2011.
- [8] O. Bingöl and S. Paçacı, "A virtual laboratory for neural network controlled DC motors based on a DC-DC buck converter," *International Journal of Engineering Education*, vol. 28, no. 3, pp. 713–723, 2012.
- [9] H. Sira-Ramírez and M. A. Oliver-Salazar, "On the robust control of buck-converter DC-motor combinations," *IEEE Transactions on Power Electronics*, vol. 28, no. 8, pp. 3912–3922, 2013.
- [10] F. E. Hoyos, A. Rincón, J. A. Taborda, N. Toro, and F. Angulo, "Adaptive quasi-sliding mode control for permanent magnet DC motor," *Mathematical Problems in Engineering*, vol. 2013, Article ID 693685, 12 pages, 2013.
- [11] F. E. Hoyos-Velasco, J. E. Candelo-Becerra, and A. Rincón-Santamaría, "Dynamic analysis of a permanent magnet DC motor using a buck converter controlled by ZAD-FPIC," *Energies*, vol. 11, no. 12, p. 3388, 2018.
- [12] F. E. Hoyos, J. E. Candelo-Becerra, and C. I. Hoyos-Velasco, "Application of zero average dynamics and fixed point induction control techniques to control the speed of a DC motor with a buck converter," *Applied Sciences*, vol. 10, no. 5, p. 1807, 2020.
- [13] F. E. Hoyos, J. E. Candelo-Becerra, and A. Rincón, "Zero average dynamic controller for speed control of DC motor," *Applied Sciences*, vol. 11, no. 12, p. 5608, 2021.
- [14] R. Silva-Ortigoza, J. R. García-Sánchez, J. M. Alba-Martínez et al., "Two-stage control design of a buck converter/DC motor system without velocity measurements via a Σ - Δ -modulator," *Mathematical Problems in Engineering*, vol. 2013, Article ID 929316, 11 pages, 2013.
- [15] R. Silva-Ortigoza, C. Márquez-Sánchez, F. Carrizosa-Corral, M. Antonio-Cruz, J. M. Alba-Martínez, and G. Saldaña-González, "Hierarchical velocity control based on differential flatness for a DC/DC buck converter-DC motor system," *Mathematical Problems in Engineering*, vol. 2014, Article ID 912815, 12 pages, 2014.
- [16] R. Silva-Ortigoza, V. M. Hernández-Guzmán, M. Antonio-Cruz, and D. Muñoz-Carrillo, "DC/DC buck power converter as a smooth starter for a DC motor based on a hierarchical control," *IEEE Transactions on Power Electronics*, vol. 30, no. 2, pp. 1076–1084, 2015.
- [17] G. K. Srinivasan and H. T. Srinivasan, "Sensorless load torque estimation and passivity based control of buck converter fed DC motor," *Science World Journal*, vol. 2015, Article ID 132843, 15 pages, 2015.
- [18] G. Rigatos, P. Siano, P. Wira, and M. Sayed-Mouchaweh, "Control of DC-DC converter and DC motor dynamics using

- differential flatness theory,” *Intelligent Industrial Systems*, vol. 2, no. 4, pp. 371–380, 2016.
- [19] G. Rigatos, P. Siano, S. Ademi, and P. Wira, “Flatness-based control of DC-DC converters implemented in successive loops,” *Electric Power Components and Systems*, vol. 46, no. 6, pp. 673–687, 2018.
- [20] F. Wei, P. Yang, and W. Li, “Robust adaptive control of DC motor system fed by buck converter,” *International Journal of Control, Automation, and Systems*, vol. 7, no. 10, pp. 179–190, 2014.
- [21] V. M. Hernández-Guzmán, R. Silva-Ortigoza, and D. Muñoz-Carrillo, “Velocity control of a brushed DC-motor driven by a DC to DC buck power converter,” *International Journal of Innovative, Computing, Information and Control*, vol. 11, no. 2, pp. 509–521, 2015.
- [22] S. Khubalkar, A. Chopade, A. Junghare, M. Aware, and S. Das, “Design and realization of stand-alone digital fractional order PID controller for buck converter fed DC motor,” *Circuits, Systems, and Signal Processing*, vol. 35, no. 6, pp. 2189–2211, 2016.
- [23] S. W. Khubalkar, A. S. Junghare, M. V. Aware, A. S. Chopade, and S. Das, “Demonstrative fractional order—PID controller based DC motor drive on digital platform,” *ISA Transactions*, vol. 82, pp. 79–93, 2018.
- [24] T. K. Nizami, A. Chakravarty, and C. Mahanta, “Design and implementation of a neuro-adaptive backstepping controller for buck converter fed PMDC-motor,” *Control Engineering Practice*, vol. 58, pp. 78–87, 2017.
- [25] M. I. F. M. Hanif, M. H. Suid, and M. A. Ahmad, “A piecewise affine PI controller for buck converter generated DC motor,” *International Journal of Power Electronics and Drive Systems*, vol. 10, no. 3, pp. 1419–1426, 2019.
- [26] J. Yang, H. Wu, L. Hu, and S. Li, “Robust predictive speed regulation of converter-driven DC motors via a discrete-time reduced-order GPIO,” *IEEE Transactions on Industrial Electronics*, vol. 66, no. 10, pp. 7893–7903, 2019.
- [27] M. G. Kazemi and M. Montazeri, “Fault detection of continuous time linear switched systems using combination of bond graph method and switching observer,” *ISA Transactions*, vol. 94, pp. 338–351, 2019.
- [28] G. Rigatos, P. Siano, and M. Sayed-Mouchaweh, “Adaptive neurofuzzy H-infinity control of DC–DC voltage converters,” *Neural Computing and Applications*, vol. 32, no. 7, pp. 2507–2520, 2020.
- [29] A. Rauf, S. Li, R. Madonski, and J. Yang, “Continuous dynamic sliding mode control of converter-fed DC motor system with high order mismatched disturbance compensation,” *Transactions of the Institute of Measurement and Control*, vol. 42, no. 14, pp. 2812–2821, 2020.
- [30] E. Guerrero, E. Guzmán, J. Linares, A. Martínez, and G. Guerrero, “FPGA-based active disturbance rejection velocity control for a parallel DC/DC buck converter-DC motor system,” *IET Power Electronics*, vol. 13, no. 2, pp. 356–367, 2020.
- [31] M. R. Stanković, R. Madonski, S. Shao, and D. Mikluc, “On dealing with harmonic uncertainties in the class of active disturbance rejection controllers,” *International Journal of Control*, vol. 94, no. 10, pp. 2795–2810, 2020.
- [32] G. K. Srinivasan, H. T. Srinivasan, and M. Rivera, “Sensitivity analysis of exact tracking error dynamics passive output control for a flat/partially flat converter systems,” *Electronics*, vol. 9, no. 11, p. 1942, 2020.
- [33] R. Madonski, K. Łakomy, M. Stankovic, S. Shao, J. Yang, and S. Li, “Robust converter-fed motor control based on active rejection of multiple disturbances,” *Control Engineering Practice*, vol. 107, Article ID 104696, 2021.
- [34] M. D. Patil, K. Vadirajacharya, and S. W. Khubalkar, “Design and tuning of digital fractional-order PID controller for permanent magnet DC motor,” *IETE Journal of Research*, 2021.
- [35] A. Rauf, M. Zafran, A. Khan, and A. R. Tariq, “Finite-time nonsingular terminal sliding mode control of converter-driven DC motor system subject to unmatched disturbances,” *International Transactions on Electrical Energy Systems*, Article ID e13070, 2021.
- [36] R. Silva-Ortigoza, J. N. Alba-Juárez, J. R. García-Sánchez, M. Antonio-Cruz, V. M. Hernández-Guzmán, and H. Taud, “Modeling and experimental validation of a bidirectional DC/DC buck power electronic converter–DC motor system,” *IEEE Latin America Transactions*, vol. 15, no. 6, pp. 1043–1051, 2017.
- [37] R. Silva-Ortigoza, J. N. Alba-Juárez, J. R. García-Sánchez, V. M. Hernández-Guzmán, C. Y. Sosa-Cervantes, and H. Taud, “A sensorless passivity-based control for the DC/DC buck converter–inverter–DC motor system,” *IEEE Latin America Transactions*, vol. 14, no. 10, pp. 4227–4234, 2016.
- [38] E. Hernández-Márquez, J. R. García-Sánchez, R. Silva-Ortigoza et al., “Bidirectional tracking robust controls for a DC/DC buck converter-DC motor system,” *Complexity*, vol. 2018, Article ID 1260743, 10 pages, 2018.
- [39] X. Chi, S. Quan, J. Chen, Y.-X. Wang, and H. He, “Proton exchange membrane fuel cell-powered bidirectional DC motor control based on adaptive sliding-mode technique with neural network estimation,” *International Journal of Hydrogen Energy*, vol. 45, no. 39, pp. 20282–20292, 2020.
- [40] A. A. A. Ismail and A. Elnady, “Advanced drive system for DC motor using multilevel DC/DC buck converter circuit,” *IEEE Access*, vol. 7, pp. 54167–54178, 2019.
- [41] J. Linares-Flores, J. Reger, and H. Sira-Ramírez, “Load torque estimation and passivity-based control of a boost-converter/DC-motor combination,” *IEEE Transactions on Control Systems Technology*, vol. 18, no. 6, pp. 1398–1405, 2010.
- [42] A. T. Alexandridis and G. C. Konstantopoulos, “Modified PI speed controllers for series-excited DC motors fed by DC/DC boost converters,” *Control Engineering Practice*, vol. 23, pp. 14–21, 2014.
- [43] S. Malek, “A new nonlinear controller for DC-DC boost converter fed DC motor,” *International Journal of Power Electronics*, vol. 7, no. 1-2, pp. 54–71, 2015.
- [44] G. C. Konstantopoulos and A. T. Alexandridis, “Enhanced control design of simple DC-DC boost converter-driven DC motors: analysis and implementation,” *Electric Power Components and Systems*, vol. 43, no. 17, pp. 1946–1957, 2015.
- [45] P. Mishra, A. Banerjee, M. Ghosh, and C. B. Baladhandautham, “Digital pulse width modulation sampling effect embodied steady-state time-domain modeling of a boost converter driven permanent magnet DC brushed motor,” *International Transactions on Electrical Energy Systems*, vol. 31, no. 8, Article ID e12970, 2021.
- [46] V. H. García-Rodríguez, R. Silva-Ortigoza, E. Hernández-Márquez, J. R. García-Sánchez, and H. Taud, “DC/DC boost converter-inverter as driver for a DC motor: modeling and experimental verification,” *Energies*, vol. 11, no. 8, p. 2044, 2018.
- [47] R. Silva-Ortigoza, V. H. García-Rodríguez, E. Hernández-Márquez et al., “A trajectory tracking control for a boost converter-inverter-DC motor combination,” *IEEE Latin America Transactions*, vol. 16, no. 4, pp. 1008–1014, 2018.

- [48] J. R. García-Sánchez, E. Hernández-Márquez, J. Ramírez-Morales et al., "A robust differential flatness-based tracking control for the "MIMO DC/DC boost converter-inverter-DC motor" system: experimental results," *IEEE Access*, vol. 7, pp. 84497–84505, 2019.
- [49] Y. Sönmez, M. Dursun, U. Güvenç, and C. Yilmaz, "Start up current control of buck-boost converter-fed serial DC motor," *Pamukkale University Journal of Engineering Sciences*, vol. 15, no. 2, pp. 278–283, 2009.
- [50] J. Linares-Flores, J. L. Barahona-Avalos, H. Sira-Ramírez, and M. A. Contreras-Ordaz, "Robust passivity-based control of a buck-boost-converter/DC-motor system: an active disturbance rejection approach," *IEEE Transactions on Industry Applications*, vol. 48, no. 6, pp. 2362–2371, 2012.
- [51] E. Hernández-Márquez, R. Silva-Ortigoza, J. R. García-Sánchez, V. H. García-Rodríguez, and J. N. Alba-Juárez, "A new "DC/DC buck-boost converter-DC motor" system: modeling and experimental validation," *IEEE Latin America Transactions*, vol. 15, no. 11, pp. 2043–2049, 2017.
- [52] E. Hernández-Márquez, R. Silva-Ortigoza, J. R. García-Sánchez, M. Marcelino-Aranda, and G. Saldaña-González, "A DC/DC buck-boost converter-inverter-DC motor system: sensorless passivity-based control," *IEEE Access*, vol. 6, pp. 31486–31492, 2018.
- [53] E. Hernández-Márquez, C. A. Avila-Rea, J. R. García-Sánchez et al., "Robust tracking controller for a DC/DC buck-boost converter-inverter-DC motor system," *Energies*, vol. 11, no. 10, p. 2500, 2018.
- [54] M. R. Ghazali, M. A. Ahmad, and R. M. T. Raja-Ismail, "Adaptive safe experimentation dynamics for data-driven neuroendocrine-PID control of MIMO systems," *IETE Journal of Research*, 2019.
- [55] E. E. Jiménez-Toribio, A. A. Labour-Castro, F. Muñoz-Rodríguez, H. R. Pérez-Hernández, and E. I. Ortiz-Rivera, "Sensorless control of sepic and cuk converters for DC motors using solar panels," in *Proceedings of the IEEE International Electric Machines and Drives Conference*, pp. 1503–1510, Miami, FL, USA, May 2009.
- [56] J. Linares-Flores, H. Sira-Ramírez, E. F. Cuevas-López, and M. A. Contreras-Ordaz, "Sensorless passivity based control of a DC motor via a solar powered sepic converter-full bridge combination," *Journal of Power Electronics*, vol. 11, no. 5, pp. 743–750, 2011.
- [57] M. H. Arshad and M. A. Abido, "Hierarchical control of DC motor coupled with cuk converter combining differential flatness and sliding mode control," *Arabian Journal for Science and Engineering*, vol. 46, pp. 9413–9422, 2021.
- [58] G. K. Srinivasan, H. T. Srinivasan, and M. Rivera, "Low-cost implementation of passivity-based control and estimation of load torque for a luo converter with dynamic load," *Electronics*, vol. 9, no. 11, p. 1914, 2020.
- [59] K. K. Chittibabu and N. K. Alphonse, "Analysis of conducted EMI with a standalone solar-powered DC motor," *Turkish Journal of Electrical Engineering & Computer Sciences*, vol. 21, no. 5, pp. 1260–1271, 2013.
- [60] L. Gil-Antonio, B. Saldivar, O. Portillo-Rodríguez, G. Vázquez-Guzmán, and S. M. De Oca-Armeaga, "Trajectory tracking control for a boost converter based on the differential flatness property," *IEEE Access*, vol. 7, pp. 63437–63446, 2019.
- [61] A. Narendra, N. V. Naik, A. K. Panda, and N. Tiwary, "A comprehensive review of PV driven electrical motors," *Solar Energy*, vol. 195, pp. 278–303, 2020.
- [62] M. Fliess, J. Lévine, P. Martin, and P. Rouchon, "Flatness and defect of non-linear systems: introductory theory and examples," *International Journal of Control*, vol. 61, no. 6, pp. 1327–1361, 1995.
- [63] R. Kumar and B. Singh, "BLDC motor driven solar PV array fed water pumping system employing zeta converter," *IEEE Transactions on Industry Applications*, vol. 52, no. 3, pp. 2315–2322, 2016.
- [64] R. Kumar and B. Singh, "Single stage solar PV fed brushless DC motor driven water pump," *IEEE Journal of Emerging and Selected Topics in Power Electronics*, vol. 5, no. 3, pp. 1377–1385, 2017.
- [65] R. Madonski, K. Łakomy, and J. Yang, "Simplifying ADRC design with error-based framework: case study of a DC-DC buck power converter," *Control Theory and Technology*, vol. 19, no. 1, pp. 94–112, 2021.
- [66] K. Łakomy, R. Madonski, B. Dai et al., "Active disturbance rejection control design with suppression of sensor noise effects in application to DC-DC buck power converter," *IEEE Transactions on Industrial Electronics*, 2021.